


RESEARCH



MEAs-Filter: a novel filter framework utilizing evolutionary algorithms for cardiovascular diseases diagnosis

Fangfang Zhu^{1,2}, Ji Ding³, Xiang Li¹, Yuer Lu⁴, Xiao Liu⁵, Frank Jiang⁵, Qi Zhao^{6*} , Honghong Su^{3*} and Jianwei Shuai^{4*}

Abstract

Cardiovascular disease management often involves adjusting medication dosage based on changes in electrocardiogram (ECG) signals' waveform and rhythm. However, the diagnostic utility of ECG signals is often hindered by various types of noise interference. In this work, we propose a novel filter based on a multi-engine evolution framework named MEAs-Filter to address this issue. Our approach eliminates the need for predefined dimensions and allows adaptation to diverse ECG morphologies. By leveraging state-of-the-art optimization algorithms as evolution engine and incorporating prior information inputs from classical filters, MEAs-Filter achieves superior performance while minimizing order. We evaluate the effectiveness of MEAs-Filter on a real ECG database and compare it against commonly used filters such as the Butterworth, Chebyshev filters, and evolution algorithm-based (EA-based) filters. The experimental results indicate that MEAs-Filter outperforms other filters by achieving a reduction of approximately 30% to 60% in terms of the loss function compared to the other algorithms. In denoising experiments conducted on ECG waveforms across various scenarios, MEAs-Filter demonstrates an improvement of approximately 20% in signal-to-noise (SNR) ratio and a 9% improvement in correlation. Moreover, it does not exhibit higher losses of the R-wave compared to other filters. These findings highlight the potential of MEAs-Filter as a valuable tool for high-fidelity extraction of ECG signals, enabling accurate diagnosis in the field of cardiovascular diseases.

Keywords: Electrocardiogram, Evolution algorithm, Filter, Noise interference, Disease diagnosis

Introduction

ECG waveforms serve as a computer-based tool for analyzing heart activity and diagnosing cardiovascular diseases [1], as well as providing valuable insights for determining medication recommendations [2, 3]. Accurate analysis of ECG parameters, including RR intervals and clarity of the P wave, plays a pivotal role in assessing heart recovery and guiding decisions regarding

medication dosage. By closely examining these ECG features, healthcare professionals can make well-informed decisions regarding the optimal dosage of cardiac-related drugs, thereby optimizing therapeutic outcomes for patients with cardiovascular diseases. Unfortunately, ECG signals are susceptible to corruption during the recording process due to various interferences, such as noise originating from electrical instruments, electrode misplacement, electromyographic (EMG) noise, or muscle artifacts [4]. The presence of such interference compromises the integrity of ECG, making accurate interpretation of cardiac conditions challenging. For example, baseline drift distorts ST segments and other low-frequency components of ECG signals. The frequency noise component of the power lines can cause distortion of ECG morphological features. EMG noise is distributed from 0.01 to 100 Hz and can cause local

*Correspondence: zhaqiqi@lnu.edu.cn; suhonghong@tsinghua-zj.edu.cn; shuaijw@ucas.ac.cn

³ Yangtze Delta Region Institute of Tsinghua University, Zhejiang, Jiaxing 314006, China

⁴ Wenzhou Institute and Wenzhou Key Laboratory of Biophysics, University of Chinese Academy of Sciences, Wenzhou 325001, China

⁶ School of Computer Science and Software Engineering, University of Science and Technology Liaoning, Anshan 114051, China

Full list of author information is available at the end of the article

waveform distortion of ECG signal. To mitigate this problem, filtering techniques for ECG signals have gained importance by aiming to suppress noise and enhance the characteristic waveforms present in ECG signals, ultimately improving the accuracy and reliability of cardiovascular disease diagnosis and medication dosage recommendations.

There are three categories of common filters for denoising ECG signals: frequency domain-based filters, adaptive-based filters, and convolutional network-based filters. Adaptive-based filters, like Wiener filters [5] and Kalman filters [6, 7], are suitable for handling non-stationary signals with time-varying properties. However, they come with certain limitations related to the assumed noise topography, algorithm design, parameter selection, and data requirements. Convolutional network-based filters [8, 9], on the other hand, can automatically learn the characteristics of noise through training data, allowing them to effectively filter out noise. However, this approach requires high-quality training data and well-designed models. Frequency domain-based filters, including finite impulse response (FIR) filters [10], infinite impulse response (IIR) filters [11], wavelet filters [12], are commonly used and serve as basic filters that separate the signals of interest and better represent the time-domain waveform. Overall, frequency domain filters continue to be a fundamental and widely used technique for denoising ECG signals. Moreover, they play a vital role in signal processing for diverse engineering applications, including single-cell multiomics data analysis [13], miRNA-lncRNA interaction prediction [14], and metabolite-disease association prediction [15]. Notably, FIR and IIR filters are particularly prominent in this regard.

In recent years, there has been an emergence of EA-based filter design method as a new technology in the field [16]. This approach offers an alternative to traditional frequency-domain-based filters, such as Butterworth and Chebyshev, which are designed using classic filter prototypes. Traditional filters such as the Butterworth filter exhibit small pass-band and stop-band fluctuations but have a wide transition bandwidth. Conversely, Chebyshev has narrow transition bands, but suffer from large fluctuations in the pass-band and stop-band. EA-based filters leverage the evolutionary algorithm to optimize filter parameters and generate optimal filters with minimal order. These filters can be implemented using a variety of evolutionary algorithms, such as genetic algorithm (GA) [17], simulated annealing (SA) [18], ant colony optimization (ACO) [19], particle swarm optimization (PSO) [20, 21], artificial bee colony algorithm (ABC) [22, 23], symbiotic organisms search (SOS) [24], whale optimization (WO) [25], and others.

However, it is important to note that these methods also have their own limitations. GA converges quickly but may easily get stuck in local optima and lacks effective local search abilities. PSO, WO, and SOS exhibit strong global search capabilities but are limited in terms of local fine search. ABC, on the other hand, is proficient in local fine search but has slow convergence. Additionally, while EA-based filter designs can improve performance, their improvement relative to classical filter design methods is restricted by the finite number of iterations and infinite search space. Furthermore, most EA-based filters are designed for fixed-length optimization problems, meaning that the filter order must be predetermined within a single optimization process, thus making it impractical to automatically find filters with the minimum order. Although a variable-length search method has been proposed for the PSO algorithm in [21], it is not applicable to other evaluation algorithms.

To address these challenges and offer a valuable filter tool for disease diagnosis [26] and biological analysis [27, 28], we propose a novel filter design framework called MEAs-Filter. This framework aims to provide the following key contributions:

- (1) Multi-engine evolution framework: MEAs-Filter utilizes state-of-the-art evolutionary algorithms as a powerful optimization engine to facilitate the design of filters. By integrating multiple evolutionary algorithms, each possessing unique strengths and advantages, MEAs-Filter aims to identify the most effective filter design ensuring optimal signal denoising.
- (2) Incorporating prior information: MEAs-Filter takes advantage of prior knowledge in the form of classical filter prototypes, known noisy signals, and key filter metrics. By incorporating this prior information, MEAs-Filter can significantly enhance performance, surpassing a two-fold improvement.
- (3) Variable-length optimization framework: This work introduces a variable-length optimization framework that is compatible with various evolutionary algorithms. This approach allows for designing filters with specified performance requirements in the minimum order. The incorporation of variable-length functionality enhances flexibility and adaptability during the filter design process.

This paper is structured as follows. Section II provides a brief explanation of the characteristic waves of ECG and the filter theory. The latter part of Section II outlines the algorithm framework proposed in this work and discusses the filter performance metrics. Section III presents the experimental and analytical results obtained. In

Section IV, discussion is provided, and the final section concludes the paper.

Problems and methods

ECG denoising problem

ECG-based cardiac diagnosis has become a reliable and standardized technique, following Willem Einthoven's initial extraction of the first clean ECG waveform [29]. The ECG waveform, as depicted in Fig. 1a, exhibits various features such as the P wave, QRS width, and ST segment, which serve as indicators of cardiac health and play a pivotal role in medication dosage control for heart disease treatment. Acquisition of the ECG signal involves placing electrodes on specific points of the body, typically on the chest, limbs, or both, to detect the electrical signals generated by the heart during the depolarization and repolarization of each heartbeat. However, ECG recording equipment may inadvertently capture EMG noise that covers the frequency range of 0 to 300 Hz [30]. Moreover, power frequency noise from the power supply and surrounding electromagnetic fields can interfere with the ECG signal. This noise often manifests as small periodic ripples with frequencies of 50 Hz or 60 Hz. As shown in Fig. 1b, this noise can distort the ECG waveform, posing challenges for medical professionals in accurately extracting diagnostic information from ECG. Therefore, it is crucial to extract clear and high-fidelity ECG waveforms to ensure accurate diagnosis.

IIR filter formulation problem

The IIR filter operates on the principle of a recursive difference equation, where the current output sample ($y(m)$) is determined by the current and past input samples ($x(m)$, $x(m-1)$, ...) and past output samples ($y(m-1)$, $y(m-2)$, ...). This relationship is illustrated in Fig. 2.

Mathematically, the difference equation for an IIR filter can be expressed as follows:

$$y(m) = \sum_{i=0}^L b_i \times x(m-i) - \sum_{i=1}^M a_i \times y(m-i), \quad M \geq L \quad (1)$$

where $x(m)$ and $y(m)$ are the discrete time series of the input and output signals, respectively. b and a are the forward and feedback coefficients of the filter. L represents the order of the forward feedback coefficient. M represents the order of the feedback coefficient, equal to the order of the filter.

The transfer function of an IIR digital filter can be expressed as:

$$H(z) = \sum_{j=0}^M b_j z^{-j} / (1 - \sum_{i=1}^L a_i z^{-i}) \quad (2)$$

Due to the infinite length of the impulse response in ideal filters, achieving these filters in practice is not feasible. Instead, our objective is to determine filter parameters that closely approximate the behavior of an ideal filter. Key parameters that play a crucial role in evaluating filter performance include pass-band ripple δ_p , stop-band ripple δ_s , and transition band width $\Delta\omega$. These parameters quantify the extent to which the filter behaves within

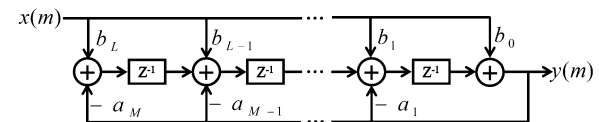


Fig. 2 Diagram illustrating the structural configuration of a typical IIR filter with $M=L$

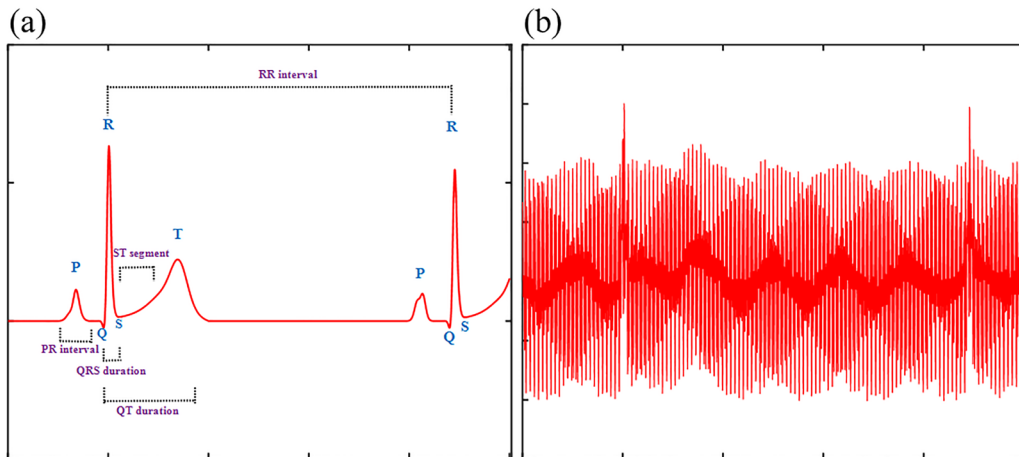


Fig. 1 ECG waveforms. **a** Clean ECG waveform. **b** ECG waveform with noise

the desired pass-band and stop-band regions, as well as the smoothness of the transition between them.

Taking a low-pass filter as an example, we can define δ_p , δ_s , and $\Delta\omega$ using Eqs. (3)–(5), respectively.

$$1 - \delta_p \leq |H(j\omega)| \leq 1 + \delta_p, |\omega| \leq \omega_c \quad (3)$$

$$|H(j\omega)| \leq \delta_s, \omega_s \leq |\omega| \leq \pi \quad (4)$$

$$\Delta\omega = \omega_s - \omega_p \quad (5)$$

where $|H(j\omega)|$ denotes the magnitude of the frequency response at angular frequency ω , ω_p and ω_s are the pass-band cutoff frequency and stop-band cutoff frequency, respectively.

When designing a filter, the goal is to find a solution (*sol*) that can meet δ_p , δ_s , ω_p and ω_s . This solution can be defined using Eq. (6).

$$\text{sol} = [n, b_0, b_1, \dots, b_M, a_1, a_2, \dots, a_L] \quad (6)$$

MEAs-Filter

MEAs-Filter proposed in this work comprises three main components: the input configuration, the optimization engine, and the result output. Figure 3a provides an illustration of these components. The input configuration

incorporates pre-design information using classical methods like Butterworth and Chebyshev filters. It also includes a training dataset with mixed signals having known noise characteristics, which can be non-stationary or non-periodic noise signals. In addition, the input configuration specifies the target objectives for filter design. The optimization engine is composed of multiple evolutionary algorithms, including PSO [31], ABC [22], SSA (sparrow search algorithm) [32], WO [25], and SOS [24]. These algorithms provide parallel searches to leverage their diverse strengths, such as global search, local search, and search efficiency. By utilizing these algorithms, a more optimal filter design can be achieved. The result output represents the filter design solutions obtained by the optimization engine based on the input configuration. Also, it should be noted that using multiple engines and pre-designed filters by classical methods increases the computational complexity of the system. However, in filter design, finding the ideal filter is prioritized over time and computational costs. Typically, filter design is conducted offline for specific scenarios and does not impact the real-time nature of the objective system. During online usage, as depicted in Fig. 3b, the mixed signal passes through an offline-designed filter based on the configuration specified in Fig. 3a. This filter effectively removes unwanted signals, resulting in a clean signal.

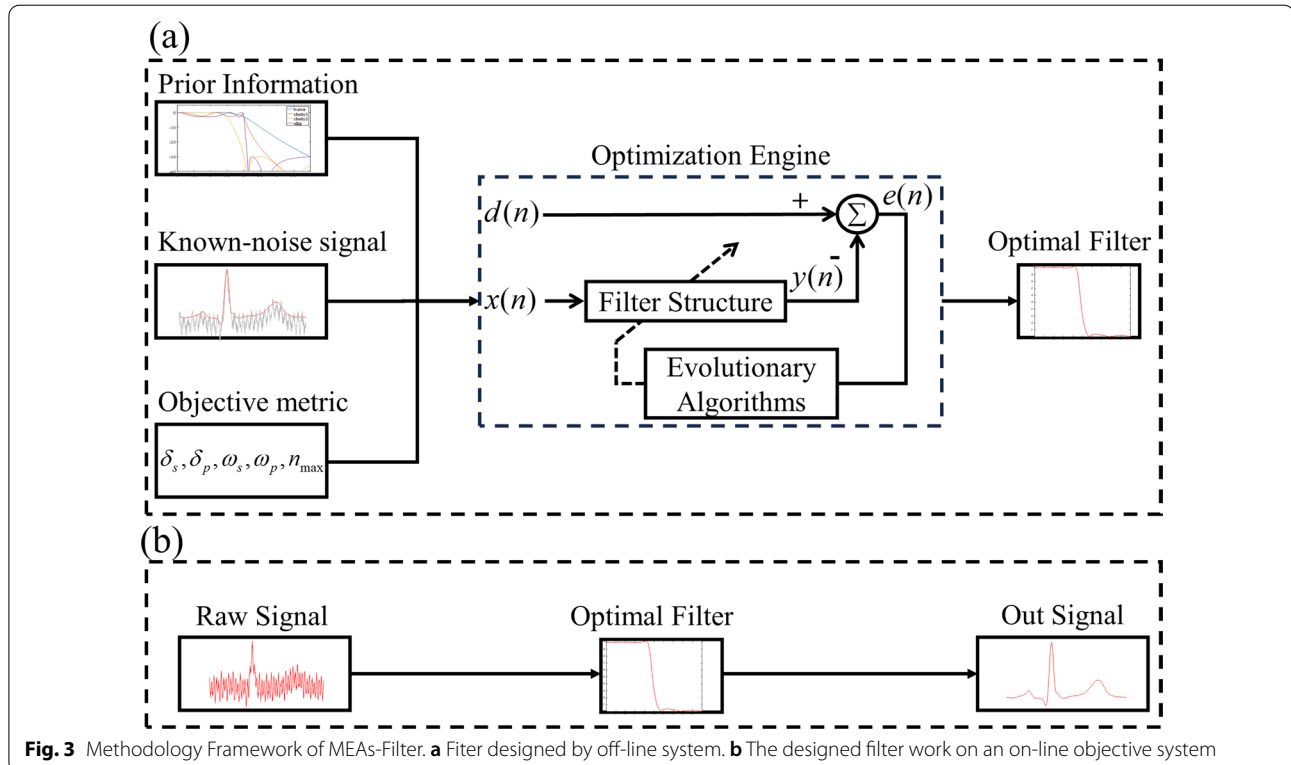


Fig. 3 Methodology Framework of MEAs-Filter. **a** Filter designed by off-line system. **b** The designed filter work on an on-line objective system

Overall, this methodology framework offers a systematic and efficient approach for filter design that effectively eliminates unwanted noise signals. It introduces a valuable tool for healthcare professionals to acquire high-fidelity ECG signals, thereby aiding in disease diagnosis.

Variable-length method

In the field of signal processing, the order of a filter plays a crucial role. Higher order leads to increased computational complexity and latency. Hence, it is essential to design a filter with the minimum order necessary to meet the specified requirements. However, traditional evolutionary algorithms are designed primarily for problems with fixed dimensions. This section proposes a method that dynamically adjusts the dimensions of the solution to find the minimum dimension that satisfies the given condition. In filter design, the number of filter coefficients can be determined based on the filter order, which directly influences the solution's dimension. By utilizing a mask model, a variable-length solution can be implemented. The mask model is used to extract the coefficients when evaluating the objective function or

$$M_a = [\alpha_1, \alpha_2, \dots, \alpha_D], \alpha_i = \begin{cases} 1, & i \in [D/2 + 2, D/2 + n + 1] \\ 0, & \text{others} \end{cases} \quad (8)$$

where M_a represents the mask used to extract the coefficient a from the solution sol , D denotes the dimension of the solution, and n represents the filter order.

The feedback coefficient b 's mask can be obtained by using Eq. (9).

$$M_b = [\beta_0, \beta_1, \beta_2, \dots, \beta_D], \beta_i = \begin{cases} 1, & i \in [2, n + 2] \\ 0, & \text{others} \end{cases} \quad (9)$$

where M_b represents the mask used to extract the coefficient b from sol .

Then the solution for variable length problems can be defined as Eq. (10). This equation differs from Eq. (6) in that it includes reserved bits and utilizes a placeholder '---'. When calculating the objective function or outputting the optimal solution, Algorithm 1 converts the solution formatted with Eq. (10) to Eq. (6).

$$sol = [n, b_0, b_1, \dots, b_M, ---, a_1, a_2, \dots, a_L, ---] \quad (10)$$

Algorithm 1 Mask-based conversion for variable length solutions

```

n = round(sol(1))
b = filterbymask(sol, M_b)
a = filterbymask(sol, M_a)
return n, b, a

```

Notes: " sol " refers to a candidate being evaluated. The " $filterbymask$ " function is used to extract specific elements based on the mask. For example, if we call the " $filterbymask$ " function with the input $sol = [5, 0.1, 0.2, 0.3, 0.4, 0.5, 0.6, 0.7]$ and $M_b = [0, 1, 1, 1, 1, 0, 0, 0]$, it will return $[0.1, 0.2, 0.3, 0.4]$.

obtaining the optimal solution. However, during the search for the optimal solution, a fixed length is utilized.

Let us define the first parameter of the solution as the filter order, denoted by n . The value of n can be determined by Eq. (7).

$$n = \text{round}(sol(1)) \quad (7)$$

where n represents the filter order, sol represents a candidate solution, round denotes the mathematical operation of rounding values to the nearest integer.

The forward coefficient a 's mask can be obtained by using Eq. (8).

The proposed variable-length approach, as described in Algorithm 1, allows the search process of the algorithm to dynamically adopt to variable-length problem. When it is necessary to compute the objective function value, a mask model is employed to transform it into a candidate solution that meets specific conditions. This approach ensures that the search procedure of the algorithm aligns accurately with the calculation of the objective function. Additionally, this method has wide applicability and can be applied to almost all evolutionary algorithms for solving variable-length problems.

Objective functions

In MEAs-Filter, the objective functions are divided into two categories: one for achieving optimal filter performance and the other for adaptive noise reduction.

Regarding filter performance, we consider three metrics: filter frequency response absolute error (FAE), δ_p and δ_s . They can be defined as follows.

$$FAE = \sum_{\omega_i} ||H(\omega_i)|| - H_d(\omega_i)|, \omega_i \in \Omega_I \quad (11)$$

$$\delta_p = \max_{\omega_i \in \Omega_p} (||H(\omega_i)|| - H_d(\omega_i)|) \quad (12)$$

$$\delta_s = \max_{\omega_i \in \Omega_s} (||H(\omega_i)||) \quad (13)$$

where $H_d(\omega_i)=1$ in pass-band, $H_d(\omega_i)=0$ in stop-band, and Ω_I denotes union of frequency bands of interest. Ω_p and Ω_s stand for pass-band and stop-band, respectively.

Regarding adaptive noise reduction, the following metrics are considered: frequency domain mean square error (FMSE), time domain mean square error (TMSE), and Pearson correlation (R). The definitions of these three metrics are provided below.

$$TMSE = \frac{1}{N} \times \sum_{i=1}^N (x_o(i) - x_d(i))^2 \quad (14)$$

$$FMSE = \frac{1}{N} \times \sum_{i=1}^N (DFT(x_o(i)) - DFT(x_d(i)))^2 \quad (15)$$

$$R = \frac{N \times \sum_{i=1}^N (x_o(i) \times x_d(i)) - \sum_{i=1}^N x_o(i) \times \sum_{i=1}^N x_d(i)}{\sqrt{N \times \sum_{i=1}^N x_d(i)^2 - (\sum_{i=1}^N x_d(i))^2} \times \sqrt{N \times \sum_{i=1}^N x_o(i)^2 - (\sum_{i=1}^N x_o(i))^2}} \quad (16)$$

where x_o and x_d denote the original ECG signal and the denoised ECG signal, respectively. DFT denotes the discrete Fourier transform of the signal x .

For the purpose of quantitative assessment, the objective function values are utilized to compare the performance of the filter. Furthermore, we have incorporated the SNR improvement metric [33] and the rate of change of R-wave amplitude ΔR_{peak} for evaluation purposes, stated as follows.

$$\Delta SNR = 10 \log_{10} \left(\frac{\sum_{i=1}^N |x_n(i) - x_o(i)|^2}{\sum_{i=1}^N |x_d(i) - x_o(i)|^2} \right) \quad (17)$$

$$\Delta R_{peak} = (R_{peak}(filtered) - R_{peak}(raw))/R_{peak}(raw) \quad (18)$$

where x_n refers to the noisy ECG signal, and $R_{peak}(filtered)$ refers to the amplitude of the R-wave after it has undergone filtering, and $R_{peak}(raw)$ denotes the amplitude of the R-wave in the original signal.

Experimental evaluation

To comprehensively evaluate the effectiveness of MEAs-Filter, two independent experiments are conducted. The primary experiment aims to validate the advantages of MEAs-Filter in filter design and compares the performance improvement of the output filter with classical methods. Additionally, an assessment is performed using the MIT-BIH arrhythmia database [34, 35] to examine the efficacy of the output filter in terms of noise reduction and fidelity as compared to classical filters. The ECG signals in this database are digitized at a rate of 360 samples per channel per second, with a resolution of 11 bits and a range of 10 millivolts. To generate noisy ECG signals, different frequency noise signals corresponding to the stop-band and transition band of the filter are introduced into the original ECG signals. These noisy signals have varying SNRs. These experiments provide comprehensive insights into the effectiveness of MEAs-Filter. Furthermore, they demonstrate its ability to reduce noise and maintain fidelity compared to classical filters.

Validation of MEAs-Filter

As mentioned above, the design and implementation of filters involve distinct procedures, with the design phase taking place offline. The primary objective is to develop high-quality filters, even if it requires additional computational time. In our work, we employ the conventional filter design method as a prior input for MEAs-Filter. Figure 4 presents a comparative analysis of three different approaches: filters designed using the traditional method, filters designed using MEAs-Filter without prior input, and filters designed using MEAs-Filter with prior input. Notably, the objective function values for these approaches are recorded as 20.17, 20.8, and 8, respectively. It is evident that the design outcome without prior input only marginally outperforms the performance achieved by the traditional filtering approach. However, when incorporating prior input into the design process,

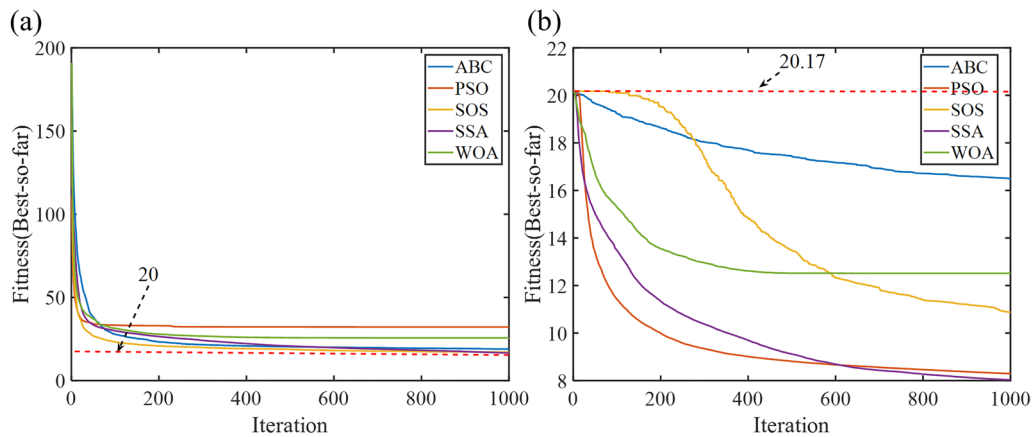


Fig. 4 Investigating the influence of prior inputs on filter performance. The red dashed line represents the objective function value of the filter designed by traditional methods. Each solid line represents an EA-based filter design. **a** SOS is selected as the output of MEAs-Filter without prior input. **b** SAA is selected as the output of MEAs-Filter with prior input

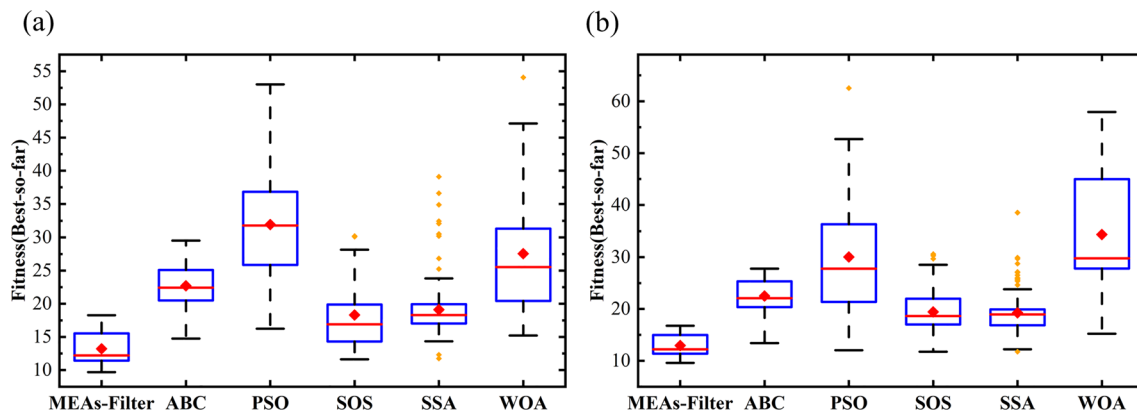


Fig. 5 Comprehensive analysis of various methods. **a** The objective function values obtained by different methods when the cutoff frequency from 0.2 to 0.8 is taken at 0.1 intervals. **b** The objective function values obtained by different methods when the cut-off frequency of the high-pass filter is taken from 0.2 to 0.8 at the interval of 0.1

a significant improvement in performance is witnessed, resulting in improvements exceeding twofold. This finding underscores the advantageous effect of utilizing prior input in the MEAs-Filter, leading to more efficient and effective filtering outcomes. By leveraging prior knowledge and information, MEAs-Filter demonstrates its ability to yield superior results.

To evaluate the robustness and sensitivity of different methods, we employ various filters as optimization objectives, including high-pass and low-pass filters with cutoff frequencies ranging from 0.2 to 0.8. Figure 5a displays the box plot for design bias when targeting low-pass filters. It is evident that MEAs-Filter exhibits the narrowest box width, indicating its superior robustness. The median design bias associated

with MEAs-Filter shows a reduction of approximately 28% to 62% compared to the other algorithms, while the mean bias is reduced by approximately 28% to 59%. In Fig. 5b, the box plot for high-pass filters reveals a similar pattern, with MEAs-Filter demonstrating a narrower box width and reductions of approximately 30% to 60% in both median and mean design bias. Ranking behind MEAs-Filter are SSA-filter and SOS-filter, they demonstrate narrow box widths but a considerable number of potential outliers. Moreover, their design bias is approximately 50% higher than that of MEAs-Filter. These results clearly demonstrate that MEAs-Filter exhibits higher robustness and smaller design bias, confirming its capability to design filters that closely approach the ideal ones.

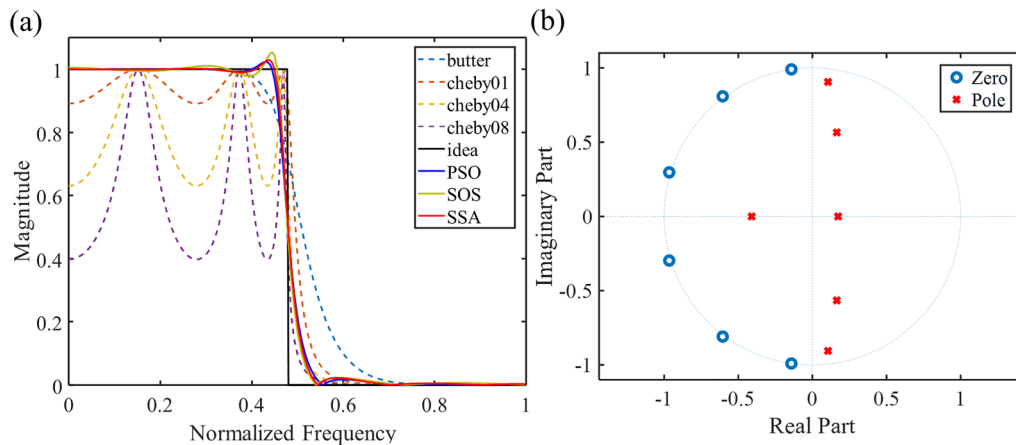


Fig. 6 Frequency response. **a** Frequency response diagram. **b** Pole-zero plot. The filters Cheby01, Cheby04, and Cheby08 correspond to Chebyshev filters with maximum pass-band ripples of 1 dB, 4 dB, and 8 dB, respectively

Table 1 Quantitative analysis of filter performance

Methods	Algorithm	δ_p	δ_s	Sum(p)	Sum(s)	Std(p)	Std(s)	$\Delta\omega$
Traditional methods	Butterworth	0.099	0.095	1.037	1.66	0.018	0.02	0.16
	cheby01	0.11	0.1	9.78	1.23	0.04	0.02	0.06
	cheby04	0.37	0.1	36.87	1.05	0.13	0.02	0.04
	cheby08	0.6	0.1	68.25	0.95	0.2	0.01	0.03
EA-based methods with Prior	ABC	0.09	0.09	0.9	6.05	0.01	0.02	0.07
	PSO	0.09	0.09	0.65	1.3	0.01	0.01	0.06
	SOS	0.09	0.09	1.47	1.82	0.01	0.01	0.05
	SSA	0.08	0.1	0.69	1.55	0.01	0.01	0.06
	WOA	0.09	0.09	1.48	1.74	0.01	0.01	0.07
EA-based methods without Prior	ABC	0.08	0.1	2.1	4.71	0.01	0.02	0.08
	PSO	0.09	0.09	5.99	2.5	0.02	0.01	0.09
	SOS	0.09	0.09	3.13	1.32	0.02	0.01	0.06
	SSA	0.09	0.1	0.91	2.83	0.01	0.02	0.08
	WOA	0.08	0.1	2.39	7.83	0.01	0.03	0.04

Bold values are pivotal in showcasing that the filter performance of the MEAs-filter design achieves a good balance in terms of transition band width, band fluctuation, and stopband attenuation, which are crucial for better recovery of physiological signals with specific characteristics

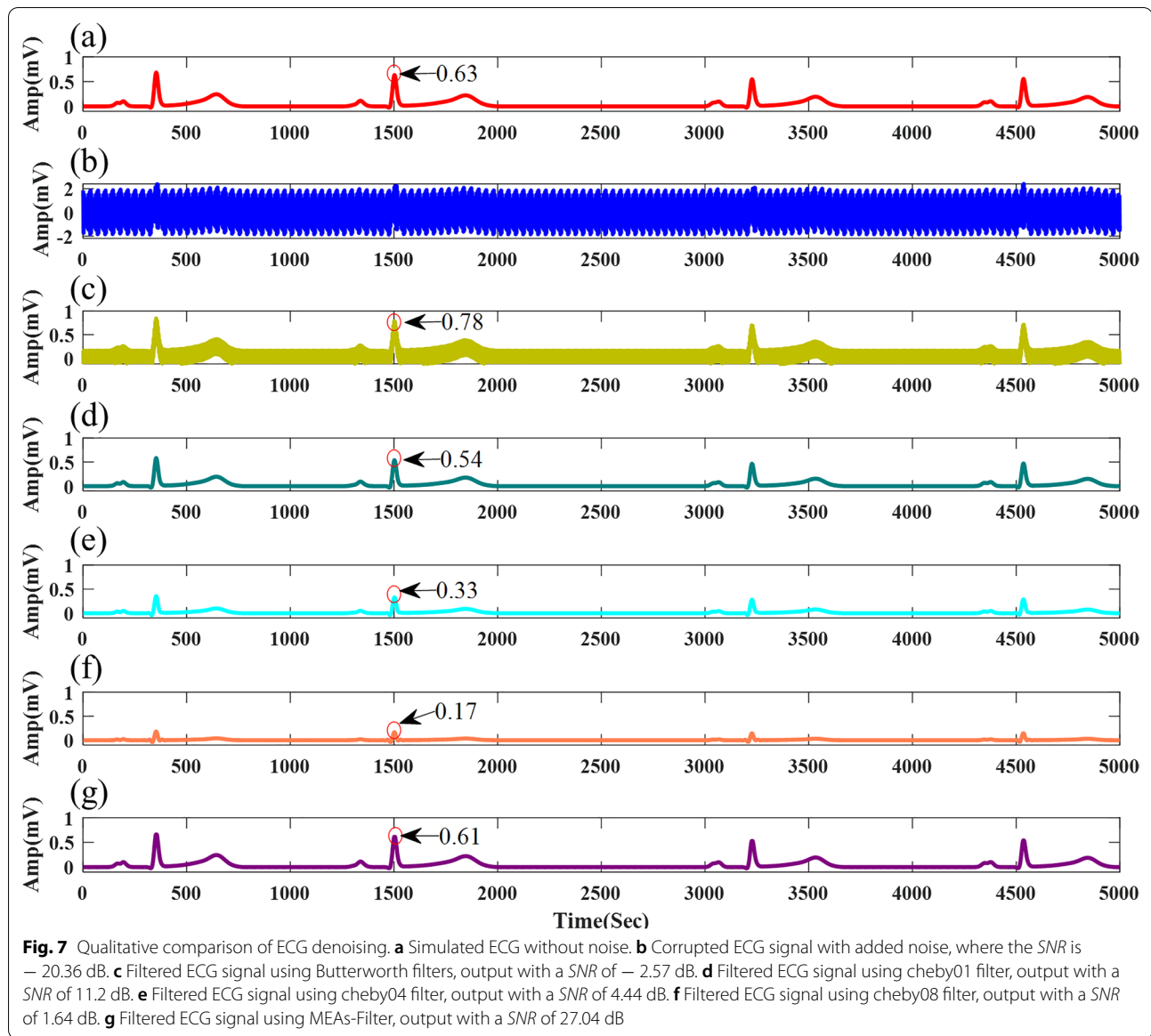
Sum(p) and Sum(s) represent the cumulative errors at each point of the filter's amplitude-frequency response in the pass-band and stop-band, respectively. Similarly, Std(p) and Std(s) represent the standard deviation of errors at each point of the filter's amplitude-frequency response in the pass-band and stop-band, respectively

Comparison of filters performance

The frequency response plot is a highly intuitive way to assess a filter's performance, while the pole-zero plot provides insights into its stability. Figure 6a illustrates the frequency response plot, showing that the Butterworth-based filter exhibits the smallest δ_p but the widest $\Delta\omega$. In contrast, the Chebyshev-based filter demonstrates the narrowest $\Delta\omega$ but experiences the largest δ_p , particularly cheby08. Moreover, the results obtained from the top three evolutionary algorithms in MEAs-Filter surpass those of traditional methods. These algorithms achieve a favorable trade-off between δ_p , δ_s , and $\Delta\omega$. Figure 6b

displays the pole-zero plot of the SSA-based filter (the top evolutionary algorithm in MEAs-Filter for this problem), revealing that all poles and zeros reside within the unit circle. This observation confirms the stability of MEAs-Filter.

Table 1 provides a comprehensive comparison of δ_p , δ_s and $\Delta\omega$ for all filters. Among these filters, MEAs-Filter demonstrates minimal values for δ_p and δ_s measuring at 0.8 and 0.09 respectively. Moreover, its $\Delta\omega$ is significantly smaller compared to the Butterworth filter. Although the SSA-based filter (which is the output of MEAs-Filter) has a slightly wider $\Delta\omega$ of 0.03 in comparison to cheby08, its



δ_p is only 13% of that exhibited by cheby08, indicating an improvement of approximately 87%. In practical engineering applications, large δ_p can result in an amplitude distortion of the original signal, which will be investigated further in the subsequent experiment.

MEAs-Filter for ECG denoising

In this section, we evaluate the effectiveness of MEAs-Filter in processing ECG signals. Our evaluation consists of both a qualitative evaluation, where the filter is applied to a simulated ECG signal, and a quantitative assessment, where real ECG signals from the MIT-BIH arrhythmia

database are subjected to varying levels of noise measured by SNR.

Figure 7a and b represent the simulated ECG signal and the ECG signal with added simulated noise, respectively. Figure 7c depicts the ECG signal post-processing with the Butterworth filter. The R-wave amplitude remains largely unaffected, however, the SNR is -2.57 dB due to the filter's limited ability to remove noise in the transition band. Moving on to Fig. 7d–f, the ECG signals processed using the Chebyshev filters exhibit SNRs of 11.2 dB, 4.44 dB, and 1.64 dB respectively. The deployment of the Chebyshev filter effectively eliminates noise and enhances the SNR, resulting in a clear visualization of the R-wave. However, the larger δ_p causes a significant

distortion in the amplitude of the R-wave, resulting in a retention of only approximately half of its original amplitude. In Fig. 7g, MEAs-Filter effectively balances δ_p and $\Delta\omega$, yielding an output SNR of 27.04 dB while maintaining a consistent R-wave amplitude comparable to the original signal. It is evident that MEAs-Filter excels at extracting high-quality ECG signals from noisy ones, making it a highly promising foundation for subsequent disease diagnosis.

A quantitative comparative analysis experiment is conducted using a real ECG signal obtained from MIT-BIH arrhythmia database. These ECGs can be categorized into four distinct classes: N (normal heartbeat), SVEB (supraventricular ectopic beat), VEB (ventricular ectopic beat), and F (fusion of ventricular and normal beat), representing different application scenarios. Denoising experiments are then performed on each category to assess the performance of different filters. In the experiment, white Gaussian noise and frequency domain noise are added to the ECG signal, resulting in a SNR ranging from -15 dB to 10 dB. Figure 8 illustrates the restoration level of denoised signals using different filters for various ECGs. The denoising effectiveness is evaluated based on three metrics: SNR improvement, R between denoised and original ECG waveforms, and ΔR_{peak} values. Figure 8a to c, d to f, g to i, and j to l correspond to N, SVEB, VEB, and F categories, respectively. The results indicate that different algorithms exhibit similar performance when applied to different categorized ECG signals. This can be attributed to the fact that these filters are specifically designed to target and eliminate specific types of noise, resulting in relatively stable and consistent filter efficiency. However, as shown in Fig. 8a, d, g, and j, MEAs-Filter leads to a significant improvement in SNR compared to other filters. Notably, it demonstrates an approximately 20% improvement in SNR compared to the second-ranked Butterworth filter. Furthermore, Fig. 8b, e, h, and k illustrate that ECG waveform obtained through the implementation of MEAs-Filter consistently exhibits a strong correlation with the original ECG waveform. Specifically, MEAs-Filter promises a 95% correlation between the filtered waveform and the original waveform, an approximately 9% improvement compared to other filters. This favorable outcome can be attributed to the smaller δ_p and narrower $\Delta\omega$ of MEAs-Filter. In contrast, the Butterworth filter, due to its wider $\Delta\omega$, fails to provide sufficient noise suppression and results in inferior improvements in SNR and waveform correlation metrics compared to the Chebyshev method and MEAs-Filter. To evaluate the effectiveness of waveform restoration, we calculate the rates of change of the R-wave peak amplitude. As depicted in Fig. 8c, f, i, and l, both the MEAs-Filter and the Butterworth filter, characterized by

smaller δ_p , successfully preserve the integrity of the filtered ECG signal with minimal distortion. On the other hand, the Chebyshev filter exhibits varying degrees of distortion on the R-wave amplitude owing to larger δ_p . Overall, the experimental analysis confirms the superior performance of MEAs-Filter in enhancing SNR, preserving waveform correlation, and maintaining high-fidelity ECG waveform across various ECG scenarios.

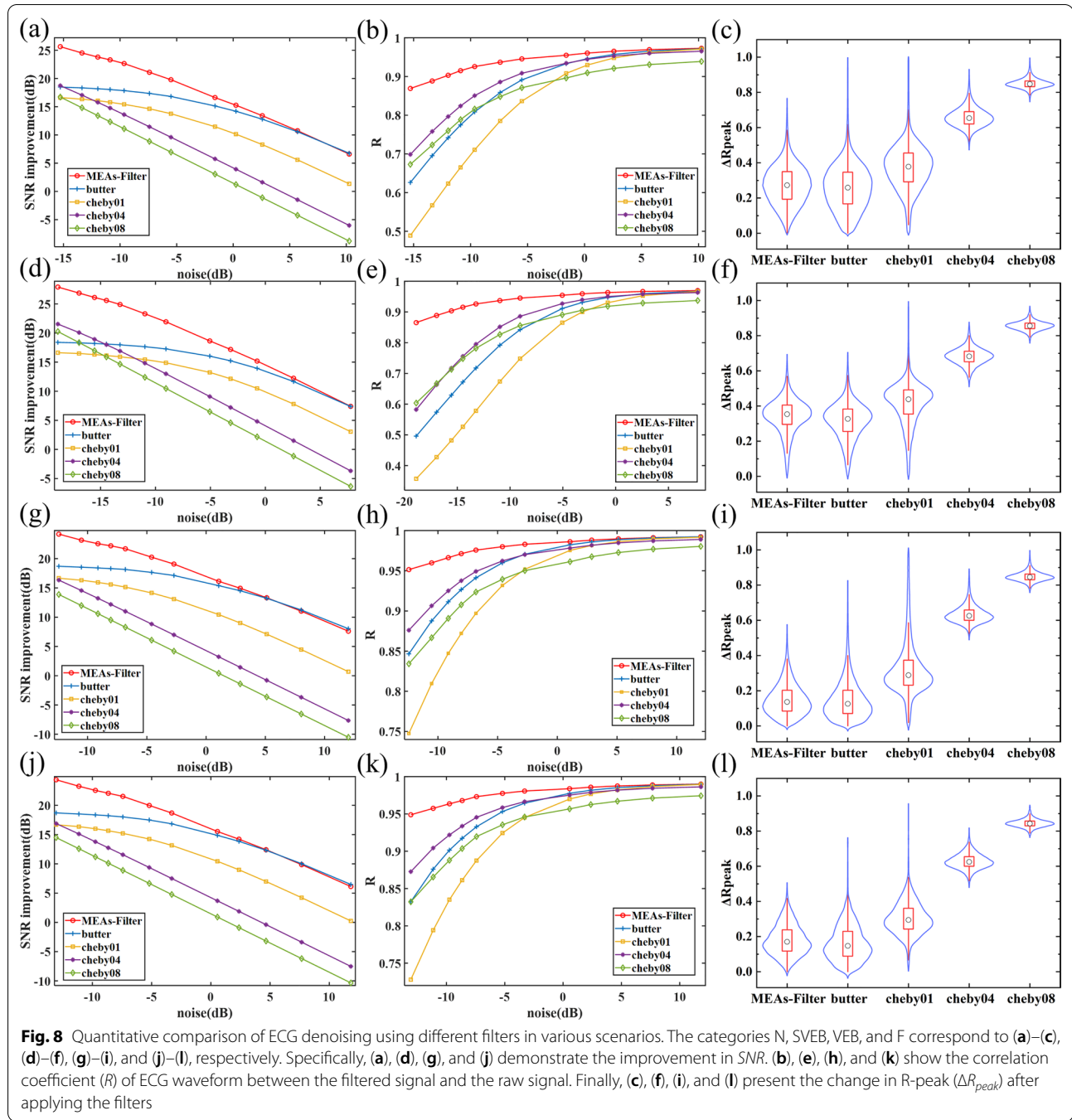
Discussion

Traditional filter design methods, such as Butterworth and Chebyshev, have limitations in achieving a balanced trade-off between pass-band ripple, stop-band attenuation, and transition band width with a limited order. In contrast, MEAs-Filter introduces an effective filter design approach that leverages evolution algorithms along with prior information. This approach demonstrates effectiveness in achieving balanced performance across three metrics while maintaining filter stability. Although adopting a multi-engine strategy and utilizing prior knowledge increase computational complexity and time during the offline filter design process, the primary objective is to obtain the most suitable filter. Therefore, MEAs-Filter in this work presents a novel and feasible solution.

The presence of pass-band ripple in a filter can lead to waveform distortion and variations in signal amplitude at different frequencies. Furthermore, a wider transition band can limit the filter's ability to eliminate noise frequencies close to the signal frequencies, particularly if they fall within the transition band. Figures 7 and 8 clearly depict these challenges. However, MEAs-Filter effectively addresses these issues by striking a balance between pass-band ripple, transition band width, and stop-band attenuation. As a result, it can remove noise while preserving the integrity of useful signals with high fidelity. This capability is crucial for accurately diagnosing cardiovascular diseases using ECG signals.

Conclusions

The proposed MEAs-Filter for designing filters using multi-evolutionary algorithms demonstrates promising results in effectively filtering noise signals and capturing the desired ECG signal. By incorporating prior knowledge from traditional filter design methods and leveraging multi-engine technology, MEAs-Filter aims to achieve a harmonious balance between pass-band ripple, stop-band attenuation, and transition band width. The verification results obtained from ECG data sets indicate that the filters designed by MEAs-Filter excel at reducing the distortion of the amplitude through minimal pass-band ripple while accurately eliminating unwanted periodic signals with narrow



transition bands. The findings underscore the potential of this design method in creating ideal filters that contribute to obtaining clearer and higher-fidelity ECG signals. MEAs-Filter can serve as valuable tools for clinical diagnosis and drug control, providing essential capabilities for ECG signal restoration.

However, there are still areas for further improvement and research. First, the design of objective function determines whether the filter output meets the engineering requirements. Therefore, further research is needed to enhance the design of objective functions. Second, MEAs-Filter mainly focuses on improving traditional frequency filters, which have relatively limited capabilities in handling random noise. This aspect can

be a key consideration for future research. Finally, the selection of evolutionary algorithms is also an important area for future investigations as they determine the core engine of filter design.

Funding

This work is supported by the Ministry of Science and Technology of the People's Republic of China (STI2030-Major Projects2021ZD0201900), National Natural Science Foundation of China (Grant No. 12090052), Foundation of Education Department of Liaoning Province (Grant No. LJKZ0280), Natural Science Foundation of Liaoning Province (Grant No. 2023-MS-288), Fundamental Research Funds for the Central Universities (Grant No. 20720230017), and Basic Public Welfare Research Program of Zhejiang Province (Grant No. LGF20F030005).

Data availability

The codes are available online at <https://github.com/PHD-Fang/MEAs-Filter>.

Declarations

Conflict of interest

The authors declare that the research was conducted in the absence of any commercial or financial relationships that could be construed as a potential conflict of interest.

Author details

¹Department of Physics, and Fujian Provincial Key Laboratory for Soft Functional Materials Research, Xiamen University, Xiamen 361005, China. ²National Institute for Data Science in Health and Medicine, and State Key Laboratory of Cellular Stress Biology, Innovation Center for Cell Signaling Network, Xiamen University, Xiamen 361005, China. ³Yangtze Delta Region Institute of Tsinghua University, Zhejiang, Jiaxing 314006, China. ⁴Wenzhou Institute and Wenzhou Key Laboratory of Biophysics, University of Chinese Academy of Sciences, Wenzhou 325001, China. ⁵School of Information Technology, Faculty of Science, Engineering and Built Environment, Deakin University, Geelong, VIC, Australia. ⁶School of Computer Science and Software Engineering, University of Science and Technology Liaoning, Anshan 114051, China.

Received: 15 September 2023 Accepted: 27 December 2023

Published online: 23 January 2024

References

- Li W. Wavelets for electrocardiogram: overview and taxonomy. *IEEE Access*. 2018;7:25627–49.
- Peng T, Malik A, Trew ML. Predicting drug-mediated pro-arrhythmic effects using pre-drug electrocardiograms. *Biomed Signal Process Control*. 2021;68:102712.
- Le D, Truong S, Brijesh P, Adjero DA, Le N. sCL-ST: supervised contrastive learning with semantic transformations for multiple lead ECG arrhythmia classification. *IEEE J Biomed Health Inform*. 2023;27:2818–28.
- Singh P, Pradhan G. A new ECG denoising framework using generative adversarial network. *IEEE/ACM Trans Comput Biol Bioinf*. 2021;18:759–64.
- Smital L, Vitek M, Kozumplik J, Provaznik I. Adaptive wavelet wiener filtering of ECG signals. *IEEE Trans Biomed Eng*. 2012;60:437–45.
- Kheirati RA. Kalman filter/smoothing-based design and implementation of digital IIR filters. *Signal Process*. 2023;208:108958.
- Hesar HD, Mohebbi M. An adaptive Kalman Filter bank for ECG denoising. *IEEE J Biomed Health Inform*. 2021;25:13–21.
- Mohebbian MR, Vedaeei SS, Wahid KA, Dinh A, Marateb HR, Tavakolian K. Fetal ECG extraction from maternal ECG using attention-based CycleGAN. *IEEE J Biomed Health Inform*. 2022;26:515–26.
- Xu F, Miao D, Li W, Jin J, Liu Z, Shen C, et al. Specificity and competition of mRNAs dominate droplet pattern in protein phase separation. *Phys Rev Res*. 2023;5:023159.
- Van Alste JA, Schilder T. Removal of base-line wander and power-line interference from the ECG by an efficient FIR filter with a reduced number of taps. *IEEE Trans Biomed Eng*. 1985;BME-32:1052–60.
- Chauhan S, Singh M, Aggarwal AK. Designing of optimal digital IIR filter in the multi-objective framework using an evolutionary algorithm. *Eng Appl Artif Intell*. 2023;119:105803.
- Martínez JP, Almeida R, Olmos S, Rocha AP, Laguna P. A wavelet-based ECG delineator: evaluation on standard databases. *IEEE Trans Biomed Eng*. 2004;51:570–81.
- Zhao J, Sun J, Shuai SC, Zhao Q, Shuai J. Predicting potential interactions between lncRNAs and proteins via combined graph auto-encoder methods. *Brief Bioinform*. 2023. <https://doi.org/10.1093/bib/bbac527>.
- Wang W, Zhang L, Sun J, Zhao Q, Shuai J. Predicting the potential human lncRNA-miRNA interactions based on graph convolution network with conditional random field. *Brief Bioinform*. 2022;23:bbac463.
- Hu H, Feng Z, Lin H, Cheng J, Lyu J, Zhang Y, et al. Gene function and cell surface protein association analysis based on single-cell multiomics data. *Comput Biol Med*. 2023;157:106733.
- Agrawal N, Kumar A, Bajaj V, Singh GK. Design of digital IIR filter: a research survey. *Appl Acoust*. 2021;172:107669.
- Ng SC, Leung S-H, Chung CY, Luk A, Lau WH. The genetic search approach. A new learning algorithm for adaptive IIR filtering. *IEEE Signal Process Mag*. 1996;13:38–46.
- Chen S, Istepanian R, Luk BL. Digital IIR filter design using adaptive simulated annealing. *Digital Signal Process*. 2001;11:241–51.
- Karaboga N, Kalinli A, Karaboga D. Designing digital IIR filters using ant colony optimisation algorithm. *Eng Appl Artif Intell*. 2004;17:301–9.
- Saha S, Yangchen S, Mandal D, Kar R, Ghoshal SP. Digital stable IIR high pass filter optimization using PSO-CFIFA. 2012 IEEE symposium on humanities, science and engineering research: IEEE; 2012. p. 389–394.
- Mohammadi A, Zahiri SH, Razavi SM, Suganthan PN. Design and modeling of adaptive IIR filtering systems using a weighted sum—variable length particle swarm optimization. *Appl Soft Comput*. 2021;109:107529.
- Karaboga N, Latifoglu F. Elimination of noise on transcranial Doppler signal using IIR filters designed with artificial bee colony—ABC-algorithm. *Digit Signal Process*. 2013;23:1051–8.
- Karaboga N. A new design method based on artificial bee colony algorithm for digital IIR filters. *J Franklin Inst*. 2009;346:328–48.
- Yadav S, Saha SK, Kar R, Mandal D. Optimized adaptive noise canceller for denoising cardiovascular signal using SOS algorithm. *Biomed Signal Process Control*. 2021;69:102830.
- Yadav S, Kumar M, Yadav R, Kumar A. A novel method to design FIR digital filter using whale optimization. 2021 IEEE bombay section signature conference (IBSSC) 2021. p. 1–5.
- Gao H, Sun J, Wang Y, Lu Y, Liu L, Zhao Q, et al. Predicting metabolite–disease associations based on auto-encoder and non-negative matrix factorization. *Brief Bioinform*. 2023;bbad259.
- Li X, Zhong C-Q, Wu R, Xu X, Yang Z-H, Cai S, et al. RIP1-dependent linear and nonlinear recruitments of caspase-8 and RIP3 respectively to necro-some specify distinct cell death outcomes. *Protein Cell*. 2021;12:858–76.
- Hu H, Feng Z, Lin H, Zhao J, Zhang Y, Xu F, et al. Modeling and analyzing single-cell multimodal data with deep parametric inference. *Brief Bioinform*. 2023;24:bbad005.
- Singh N, Ayub S, Saini J. Design of digital IIR filter for noise reduction in ECG signal. 2013 5th international conference and computational intelligence and communication networks: IEEE; 2013. p. 171–176.
- Kamata K, Aho AJ, Hagihira S, Yli-Hankala A, Jäntti V. Frequency band of EMG in anaesthesia monitoring. *Br J Anaesth*. 2011;107:822–3.
- Ahirwal MK, Kumar A, Singh GK. Adaptive filtering of EEG/ERP through noise cancellers using an improved PSO algorithm. *Swarm Evol Comput*. 2014;14:76–91.
- Xue J, Shen B. A novel swarm intelligence optimization approach: sparrow search algorithm. *Syst Sci Control Eng*. 2020;8:22–34.
- Sayadi O, Shamsollahi MB. ECG denoising and compression using a modified extended Kalman filter structure. *IEEE Trans Biomed Eng*. 2008;55:2240–8.
- Goldberger AAL, Glass L, Hausdorff J, Ivanov PC, Mark R, Mietus JE, Moody GB, Peng CK, Stanley HE. PhysioBank, PhysioToolkit, and PhysioNet: Components of a new research resource for complex physiologic signals. *Circulation [Online]*. 2000;101(23):pp. e215–e220.

35. Moody GB, Mark RG. The impact of the MIT-BIH arrhythmia database. *IEEE Eng Med Biol Mag.* 2001;20:45–50.

Publisher's Note Springer Nature remains neutral with regard to jurisdictional claims in published maps and institutional affiliations.

Springer Nature or its licensor (e.g. a society or other partner) holds exclusive rights to this article under a publishing agreement with the author(s) or other rightsholder(s); author self-archiving of the accepted manuscript version of this article is solely governed by the terms of such publishing agreement and applicable law.